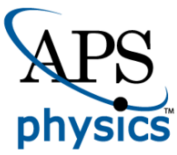

Reconfigurable Quantum-Dot Molecules Created by Atom Manipulation

Yi Pan, Jianshu Yang, Steven C. Erwin, Kiyoshi Kanisawa, and Stefan Fölsch

Phys. Rev. Lett. **115**, 076803 — Published 14 August 2015

DOI: 10.1103/PhysRevLett.115.076803

Reconfigurable quantum-dot molecules created by atom manipulation

Yi Pan[1], Jianshu Yang[1], Steven C. Erwin[2], Kiyoshi Kanisawa[3], and Stefan Fölsch[1]

[1]*Paul-Drude-Institut für Festkörperelektronik, Hausvogteiplatz 5-7, 10117 Berlin, Germany*

[2] *Center for Computational Materials Science, Naval Research Laboratory, Washington, DC 20375, USA*

[3]*NTT Basic Research Laboratories, NTT Corporation, 3-1 Morinosato Wakamiya, Atsugi, Kanagawa, 243-0198, Japan*

(Resubmitted 23 July, 2015)

Quantum-dot molecules were constructed on a semiconductor surface using atom manipulation by scanning tunneling microscopy (STM) at 5 K. The molecules consist of several coupled quantum dots, each of which comprises a chain of charged adatoms that electrostatically confines intrinsic surface-state electrons. The coupling takes place across tunnel barriers created reversibly using the STM tip. These barriers have an invariant, reproducible atomic structure and can be positioned – and repeatedly repositioned – to create a series of reconfigurable quantum-dot molecules with atomic precision.

PACS numbers: 68.37.Ef, 68.47.Fg, 73.21.La, 81.16.Ta

Quantum dots create quantized electronic states with discrete energies [1,2,3]. When two or more dots are coupled to each other, quantum tunneling can lead to the coherent superposition and entanglement of dot-confined states [4,5,6,7,8,9], a key ingredient for quantum information processing [10,11]. Coupled quantum dots – often referred to as "quantum-dot molecules" – have been created in semiconductor heterostructures using various approaches: for example, by growing vertically and laterally aligned nanocrystals [4,7,12,13] or by depleting a two-dimensional electron gas using external gates [5,6,8,9] and scanning probe-based local oxidation [14,15]. Virtually all of these approaches are constrained by two fundamental limitations. First, the quantum dots themselves inevitably have intrinsic, stochastic variations in their size and shape – and hence in their wave functions and energies. Second, the quantum-dot molecules have a "molecular structure" that is fixed at their creation and cannot be easily changed thereafter – a challenge for precision studies of how the properties of molecules evolve as their structure is systematically varied.

In this Letter we demonstrate a class of quantum-dot molecules that solve both of these problems: perfectly reproducible and easily reconfigured molecules created on a semiconductor surface using atom manipulation techniques [16] in a scanning tunneling microscope (STM). We first assembled a single long chain of ionized indium adatoms on an InAs surface. Because the adatoms are charged, the chain creates an attractive electrostatic potential well that strongly confines InAs surface-resonance electrons to quantized particle-in-a-box states. Next, we used the STM tip to create defects within the chains. These defects have a special nature that is well understood from our previous work [17]: each compensates the charge of the two adjacent adatoms, creating an electrostatic potential barrier which divides the quantum dot into smaller dots. The smaller dots are weakly coupled through the barrier to form a quantum-dot molecule

whose states are accurately described by standard molecular-orbital theory. Additional defects can be used to further subdivide the dot, forming more complex molecules. Finally, we show that the defects can be easily erased and repositioned, and hence that the molecule can be repeatedly reconfigured without repositioning any atoms. This technique establishes a versatile new approach to creating atomically precise quantum-dot molecules with widely varying yet highly reproducible properties.

We used InAs(111)A surfaces grown by molecular beam epitaxy (MBE), as described in detail in ref.(18). The investigations were carried out with an ultrahigh-vacuum (UHV) STM operated at a sample temperature of 5 K. Electrochemically etched tungsten tips were cleaned in UHV by Ne ion sputtering and electron-beam heating. To condition the final tip, current pulsing at sample bias voltages of up to 10 V was performed, followed by gentle tip-surface contact to create an atomically sharp tip. This treatment results in an agglomeration of indium at the tip apex, establishing a tip state that allows for a reliable vertical manipulation of native In adatoms on InAs(111)A. Spectroscopic measurements of the differential tunneling conductance were performed by lock-in technique (5 to 10 mV peak-to-peak modulation at a frequency of 675 Hz) with the feedback loop disabled.

Figure 1(a) illustrates the InAs(111)A surface structure with surface indium atoms (In_{surf}, green spheres) in the topmost layer and arsenic (orange) in the second layer. The (111)A termination is stabilized by a (2×2) In-vacancy reconstruction [19] with a hexagonal unit cell (gray-shaded area) and a nearest-neighbor vacancy spacing of 8.57 Å. The MBE-grown InAs(111)A surface exhibits a low concentration of native indium adatoms (In_{ad}) absorbed on the In vacancies [20]. The In_{ad} atom is positively charged, as evident from an increased apparent height around itself when imaged at positive sample bias. This signature in STM imaging arises

from the In_{ad}-induced local potential screened by conduction-band electrons as first revealed for the inverted case of acceptor-like adatoms [21]. By mapping the local electrostatic potential [22], we found that the In_{ad} donor character is consistent with a charge state +1 [17]. In addition, In_{ad} atoms are weakly bound to the surface and can be repositioned by the STM tip [18,23]. The STM topography image in Fig. 1(b) shows three In_{ad} dimers, each consisting of two adatoms positioned on nearest-neighbor vacancy sites. The surface corrugation around the dimers reflects the In_{surf} positions appearing as faint protrusions and the vacancies as depressions. The corresponding atomic arrangement is shown in Fig. 1(a) depicting the In_{ad} atoms as black spheres.

Due to the build-up of charge in a nanostructure assembled from +1 ionized In_{ad}, nearby In_{surf} atoms can become bistable in their charge state and vertical height, as previously revealed by STM and first-principles calculations [17]. For the atomic arrangement in Fig. 1, this occurs for the In_{surf} atom in the center of the structure (dashed circle). This atom is bistable, with two possible configurations: coplanar with the surface In layer as in Fig. 1(b), and "popped up" to a height close to that of the In_{ad} atoms themselves (1.7 Å) as in Fig. 1(c). In STM imaging, the popped-up In_{surf} plus the adjacent In_{ad} atoms appear as the uniform protrusion in Fig. 1(c). All three indium atoms within this defect donate an electron to the environment, but the positive charge of these donors is almost completely screened by the three donated electrons that occupy As lone-pair orbitals below the popped-up In_{surf} atom. This screening reduces the Coulomb energy of the charged nanostructure. Hence, a critical minimum size is required before the bistable behavior can result. In the dimer arrangement in Fig. 1, this criterion is fulfilled when at least three dimer units are assembled, whereas straight In_{ad} chains require at least six atoms to show bistability [17]. We note that coupled bistability in charge state and atomic configuration has been observed previously for Si impurities in the surface layer of GaAs(110) [24,25]. In that

system, the presence of the STM tip held at appropriate bias was required to stabilize one of the two observed states. In the case discussed here, however, In_{surf} atoms within an In_{ad} nanostructure can be reversibly switched via electrostatic coupling to the STM tip and then remain stable in one or the other state even without the tip [26].

To construct quantum dot molecules we consider the electrostatic potential well created by an N-atom chain of +1 ionized In adatoms at nearest-neighbor vacancy sites. This potential confines surface resonances of the pristine InAs(111)A surface, giving rise to the formation of quantized states with wave functions $\psi_n(\boldsymbol{r})$ having n lobes and $n-1$ nodes [27]. When a popped-up In_{surf} atom is formed along the chain, the resulting electrically neutral complex creates a tunnel barrier within the potential well. The upper panel of Fig. 2(a) shows the STM topography of an In_{14} chain with a barrier located in the center. The corresponding density-of-states (DOS) spatial maps in the lower panels reflect the formation of a symmetric bonding (σ) and an antisymmetric antibonding (σ^*) molecular state. This behavior is nearly equivalent to that of two In_6 chains coupled across a gap of two empty vacancy sites [27], as shown in Fig. 2(b) [28]. Figure 2(c) compares differential tunneling conductance (dI/dV) spectra of the quantum dot molecules shown in (a) and (b), revealing essentially the same σ–σ^* splitting and therefore the same coupling between the individual quantum dots. This is consistent with our assertion that the defect reflects nearly complete compensation of the positive charge of the popped-up In_{surf} atom and its two adjacent chain atoms. Within the linear-combination-of-atomic-orbitals (LCAO) description of molecular orbitals, the observed σ–σ^* splitting $\Delta = 67$ meV is equivalent to a resonance integral value of $\beta = -\Delta/2 = -33.5$ meV.

Next, we exploit the capability of precisely positioning the tunnel barrier within the chain to realize a tunable heteronuclear diatomic molecule. The topography images in Fig. 3(a) depict a

sequence of an In_{20} chain with one barrier at different locations, creating two coupled dots *A* and *B*. Starting from the homonuclear molecule (N_A,N_B)=(9,9) [top panel] the molecule is changed stepwise to the heteronuclear molecule (N_A,N_B)=(12,6). Figure 3(b) shows the corresponding DOS bias maps D(*x*,*V*) versus bias *V* and position *x* along the dashed line indicated in the top panel of Fig. 3(a). These maps reveal two resonances in the bias-dependent differential tunnel conductance associated with the σ and σ^* orbitals of the coupled dots. Upon changing the molecule from (9,9) to (12,6), the σ–σ^* splitting increases and the σ (σ^*) orbital density is transferred to the larger (smaller) dot. Within the LCAO picture of avoided crossing in a two-level system the splitting is $\Delta=\sqrt{(E_A-E_B)^2+4\beta^2}$, where $E_{A,B}$ are the ground-state energies for chains with $N_{A,B}$ atoms [29] and $\beta = -18.5$ meV was extracted from the splitting of 37 meV observed for (N_A,N_B)=(9,9). This splitting is smaller than for the molecule with (N_A,N_B)=(6,6) discussed in Fig. 2, indicating a decreasing quantum coupling with increasing $N_{A,B}$ [30]. Figure 3(c) shows that the experimental splitting Δ as a function of the energy difference (E_A–E_B) is reasonably well described by the model of avoided crossing.

This approach can be extended to more complex quantum-dot molecules. For example, a linear triatomic molecule can be formed from an In_{22} chain with two tunnel barriers created by popped In_{surf} atoms. Figure 4(a) shows an arrangement of barriers yielding three dots with the same size, (N_A,N_B,N_C)=(6,6,6). In this case, the interdot coupling leads to the formation of a molecular orbital triplet. This is apparent from the *dI/dV* resonances in Fig. 4(b) taken with the STM tip probing the confined DOS of the central dot (red) and the outer dots (green and blue) [the respective tip positions are indicated by crosses in Fig. 4(a)]. The resonances are equally separated by $\Delta = 48$ meV. For a linear triatomic molecule, this splitting is equivalent to a resonance integral of $\beta = -\Delta/\sqrt{2} = -33.9$ meV, extremely close to the value for the diatomic

molecule with (N_A,N_B)=(6,6). Figure 4(c) shows the corresponding spatial DOS maps associated with the resonances and proves that the observed state densities agree with the respective LCAO-expanded molecular orbitals. In the basis of the three dots, these are $|\sigma\rangle$=(+1,+$\sqrt{2}$,+1) for the bonding orbital (lower panel), and $|\sigma_1^*\rangle$=(+1,0,–1) and $|\sigma_2^*\rangle$=(+1,–$\sqrt{2}$,+1) for the antibonding orbitals (center and upper panel).

In summary, we created quantum dots which electrostatically confine surface resonances to form quantized electronic states. By introducing tunnel barriers within the chain, these linear dots were subdivided into smaller dots to form an artificial quantum-dot molecule of arbitrary size and complexity. The tunnel barrier is uniquely defined by the atomic structure of the associated defect, and can be created and repeatedly repositioned by the STM tip with atomic precision. In this way, highly reproducible and reconfigurable quantum dot molecules with high-fidelity, tunable electronic states could be easily constructed. Our results suggest that the tunnel barrier is switched via electrostatic coupling to the STM tip. This implies that the reconfiguration could be controlled, in principle, also by external gate electrodes, provided that future technologies will make it possible to fabricate them. The approach described here could, in principle, be extended to realize coherently coupled dot arrays in two dimensions – an important step towards the realization of artificial quantum materials with broadly variable and precisely controlled properties.

Financial support by the German Research Foundation (FO 362/4-1) is gratefully acknowledged. S.C.E. was supported by the Office of Naval Research through the Naval Research Laboratory's Basic Research Program.

References

[1] M. A. Kastner, Physics Today **46**, 24 (1993).

[2] R. C. Ashoori, Nature **379**, 413 (1996).

[3] L. P. Kouwenhoven, D. G. Austing, and S. Tarucha, Rep. Prog. Phys. **64**, 701 (2001).

[4] G. Schedelbeck, W. Wegscheider, M. Bichler, and G. Abstreiter, Science **278**, 1792 (1997).

[5] T. H. Oosterkamp, T. Fujisawa, W. G. van der Wiel, K. Ishibashi, R. V. Hijman, S. Tarucha, and L. P. Kouwenhoven, Nature **395**, 873 (1998).

[6] T. Fujisawa, T. H. Oosterkamp, W. G. van der Wiel, B. W. Broer, R. Aguado, S. Tarucha, L. P. Kouwenhoven, Science **282**, 932 (1998).

[7] M. Bayer, P. Hawrylak, K. Hinzer, S. Fafard, M. Korkusinski, Z. R. Wasilewski, O. Stern, and A. Forchel, Science **291**, 451 (2001).

[8] T. Hayashi, T. Fujisawa, H. D. Cheong, Y. H. Jeong, Y. Hirayama, Phys. Rev. Lett. **91**, 226808 (2003).

[9] A. C. Johnson, J. R. Petta, J. M. Taylor, A. Yacoby, M. D. Lukin, C. M. Marcus, M. P. Hanson, and A. C. Gossard, Nature **435**, 925 (2005).

[10] A. Ekert and R. Jozsa, Rev. Mod. Phys. **68**, 733 (1996).

[11] C. Nayak, S. H. Simon, A. Stern, M. Freedman, and S. D. Sarma, Rev. Mod. Phys. **80**, 1083 (2008).

[12] Z. R. Wasilewski, S. Fafard, J. P. McCaffrey, J. Cryst. Growth **201**, 1131 (1999).

[13] L. Wang, A. Rastelli, S. Kiravittaya, M. Benyoucef, and O. G. Schmidt, Adv. Mater. **21**, 2601 (2009).

[14] A. Fuhrer, A. Dorn, S. Lüscher, T. Heinzel, K. Ensslin, W. Wegscheider, and M. Bichler, Superlattices Microstruct. **31**, 19 (2002).

[15] M. Sigrist, T. Ihn, K. Ensslin, D. Loss, M. Reinwald, and W. Wegscheider, Phys. Rev. Lett. **96**, 036804 (2006).

[16] J. A. Stroscio and D. M. Eigler, Science **254**, 1319 (1991).

[17] J. Yang, S. C. Erwin, K. Kanisawa, C. Nacci, and S. Fölsch, Nano Lett. **11**, 2486 (2011).

[18] J. Yang, C. Nacci, J. Martínez-Blanco, K. Kanisawa, and S. Fölsch, J. Phys. Condens. Matter **24**, 354008 (2012).

[19] D. J. Chadi, Phys. Rev. Lett. **52**, 1911 (1984).

[20] T. Taguchi and K. Kanisawa, Appl. Surf. Sci. **252**, 5263 (2006).

[21] J. A. Stroscio and R. M. Feenstra, Phys. Rev. Lett. **58**, 1668 (1987).

[22] K. Teichmann, M. Wenderoth, S. Loth, R. G. Ulbrich, J. K. Garleff, A. P. Wijnheijmer, and P. M. Koenraad, Phys. Rev. Lett. **101**, 076103 (2008).

[23] S. Fölsch, J. Yang, C. Nacci, and K. Kanisawa, Phys. Rev. Lett. **103**, 096104 (2009).

[24] J. K. Garleff, A. P. Wijnheijmer, C. N. v. d. Enden, and P. M. Koenraad, Phys. Rev. B **84**, 075495 (2011).

[25] E. P. Smakman and P. M. Koenraad, J. Phys. Condens. Matter **27**, 154201 (2015).

[26] See Fig. S1 in the supplementary material.

[27] S. Fölsch, J. Martínez-Blanco, J. Yang, K. Kanisawa, and S. C. Erwin, Nat. Nanotechnol. **9**, 505 (2014).

[28] Removing and re-inserting atoms within a chain by vertical atom manipulation is not feasible: such attempts result in a degradation of the tip apex and/or the structure around the atomic gap, apparently due to strong short-range force interactions between tip and sample.

[29] See Fig. S2 in the supplementary material.

[30] See Fig. S3 in the supplementary material.

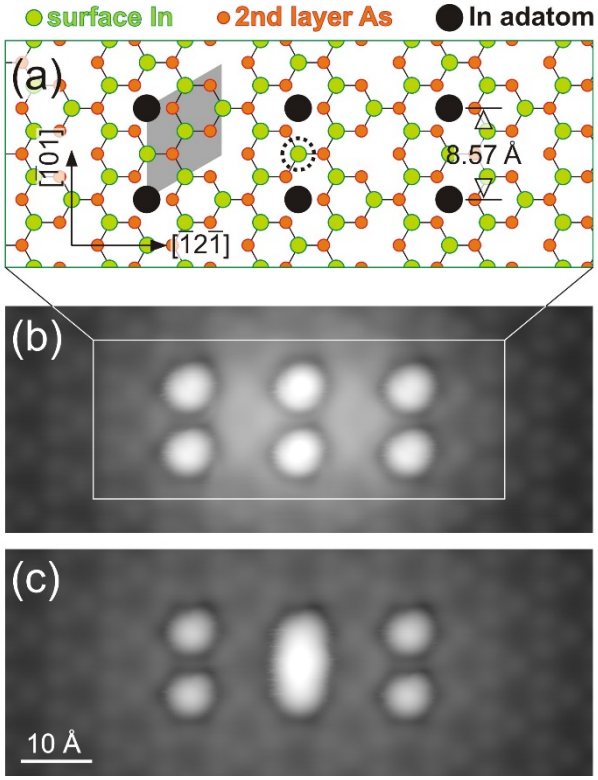

FIG. 1 (color online). (a) Model of the reconstructed InAs(111)A-(2×2) surface with indium atoms (green) in the surface layer and arsenic atoms (orange) in the second layer. The 2×2 In-vacancy reconstruction has a hexagonal unit cell (grey) with lattice vector $a' = a_0\sqrt{2}$ =8.57 Å (a_0 = 6.06 Å: cubic InAs lattice constant). (b) STM topography image (5 nA, 75 mV) of six In adatoms (In_{ad}) arranged as three dimers. Within each dimer the In_{ad} are located at neighboring In-vacancy sites, as indicated by black circles in (a). The faint increase in apparent height within the dimer structure is due to the local electrostatic potential induced by the positively charged adatoms. (c) STM image after creating a defect in the middle dimer by switching the surface In atom in the center of the structure [the circled green atom in (a)] to its metastable popped-up position. The complex consisting of the popped-up surface atom and the two adjacent In_{ad} appears as a uniform oblong protrusion.

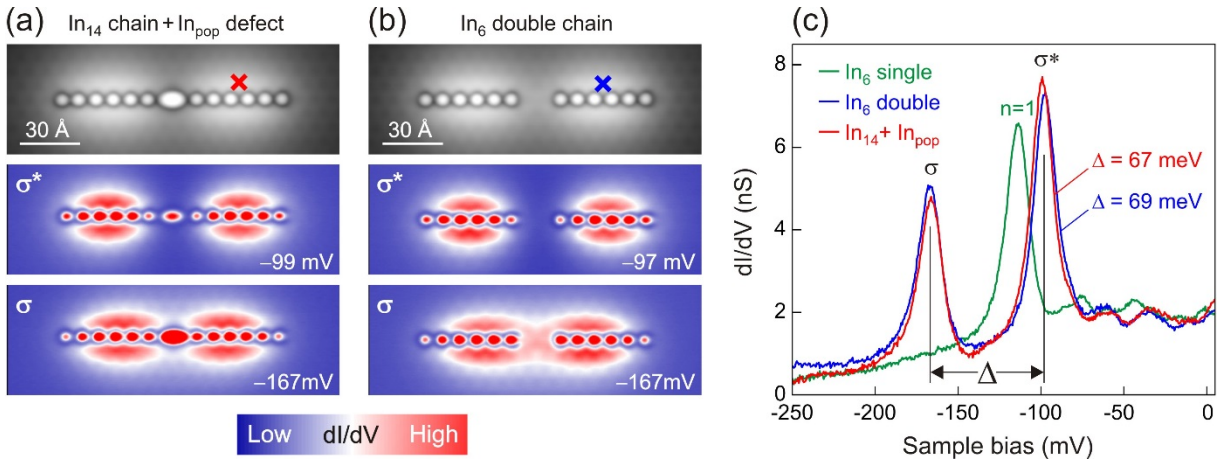

FIG. 2 (color online). (a) Top panel: STM topography image (0.1 nA, –0.3 V) of a 14-atom In_{ad} chain with a popped-up In surface atom in the center. Center and lower panel: Corresponding spatial density-of-states (DOS) maps revealing the formation of a bonding (σ, lower panel) and an antibonding state (σ*, center panel). (b) STM image of two six-atom chains separated by a gap of two empty vacancy sites, showing that the bonding and antibonding states are qualitatively very similar to the states in (a). (c) Differential conductance (*dI/dV*) spectra (red and blue curve) recorded at the positions marked by the red and blue crosses in (a) and (b), establishing the resonant character of the σ and σ* states. The σ–σ* splitting *Δ* is essentially the same for the structures in (a) and (b). For comparison, the green spectrum shows the ground state resonance (*n*=1) of a single In_6 chain.

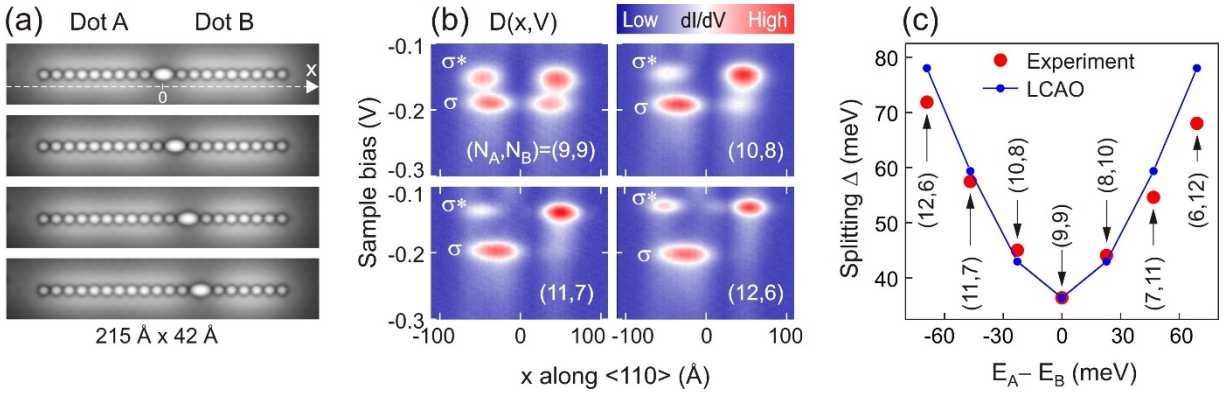

FIG. 3 (color online). (a) STM topography images (0.1 nA, –0.3 V) of a 20-atom In_{ad} chain with one popped-up In surface atom at different positions within the chain. The defect divides the In_{20} chain into two dots denoted A and B. (b) Bias and position-dependent DOS maps recorded along the x axis defined by the dashed line in (a). N_A and N_B denote the number of In_{ad} atoms within dots A and B, respectively. Starting from the symmetric case with $(N_A,N_B)=(9,9)$, the σ–σ* splitting gradually increases as the double dot is changed stepwise to $(N_A,N_B)=(12,6)$. (c) Experimental splitting (red points) for different (N_A,N_B) plotted versus the energy difference $E_A–E_B$, where E_A and E_B are the ground-state energies of single chains with N_A and N_B atoms. A simple linear-combination-of-atomic orbitals (LCAO) model for the avoided crossing in a two-level system is shown in blue for comparison.

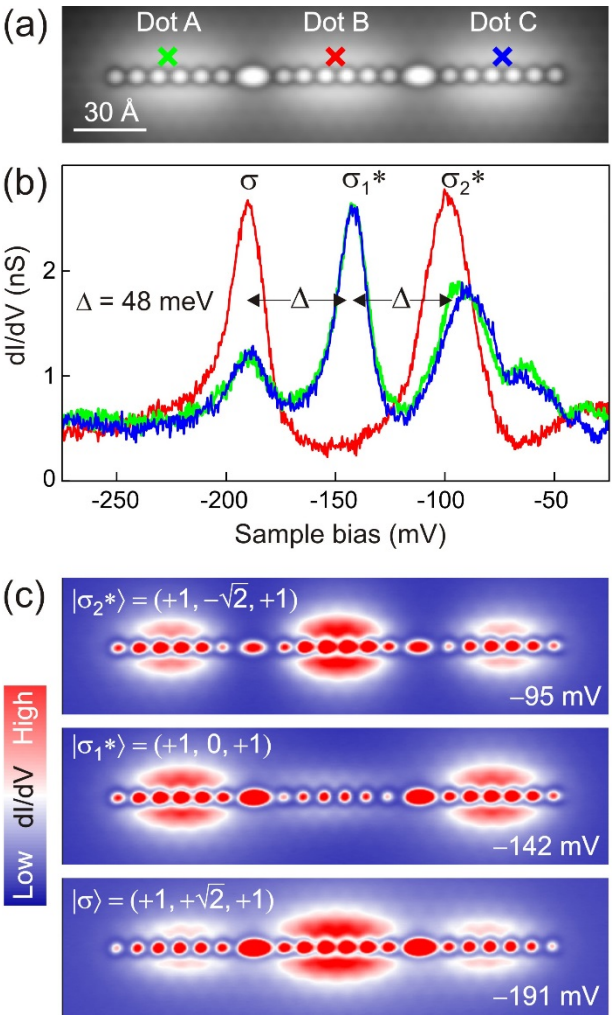

FIG. 4 (color online). (a) STM topography image (0.1 nA, –0.3 V) of a 22-atom In_{ad} chain with two popped-up In surface atoms dividing the chain into three six-atom dots A, B, and C. (b) *dI/dV* spectra taken at the positions marked by crosses in (a), revealing a triplet state with a splitting Δ=48 meV. (c) Spatial DOS maps recorded at the respective bias voltages where *dI/dV* resonances are detected in (b). The observed DOS distributions are consistent with the LCAO molecular orbitals of a linear triatomic molecule, namely $|\sigma\rangle=(+1,+\sqrt{2},+1)$ for the bonding orbital (lower panel), and $|\sigma_1^*\rangle=(+1,0,+1)$ and $|\sigma_2^*\rangle=(+1,-\sqrt{2},+1)$ for the antibonding orbitals (center and upper panel).